Coordinated Voltage Control in Unbalanced Distribution Networks with Two-stage Distributionally Robust Chance-constrained Receding Horizon Control

Zhang, Zhengfa; Silva, Filipe Miguel Faria da; Guo, Yifei; Bak, Claus Leth; Chen, Zhe

Published in:
Renewable Energy

DOI (link to publication from Publisher):
10.1016/j.renene.2022.08.086

Publication date:
2022

Document Version
Publisher's PDF, also known as Version of record

Renewable Energy 198 (2022) 907–915

Contents lists available at ScienceDirect

Renewable Energy

journal homepage: www.elsevier.com/locate/renene

Coordinated voltage control in unbalanced distribution networks with two-stage distributionally robust chance-constrained receding horizon control☆

Zhengfa Zhang [a,*], Filipe Faria da Silva [a], Yifei Guo [b], Claus Leth Bak [a], Zhe Chen [a]

[a] Department of Energy Technology, Aalborg University, Aalborg 9220, Denmark
[b] Department of Electrical and Electronic Engineering, Imperial College, London SW7 2AZ, UK

ARTICLE INFO

Keywords:
Voltage control
Distributionally robust chance-constrained
Receding horizon control
Distribution network
Distributed generation

ABSTRACT

The integration of increasing share of renewable based distributed generation in distribution networks brings great challenges to voltage control. To address this issue, this paper presents a two-stage distributionally robust chance-constrained receding horizon control algorithm. In the proposed method, the distributionally robust chance-constrained reformulation of chance-constrained voltage control is derived, which is not only accurate, but also computationally efficient. Rather than perfect knowledge about the uncertainty associated with renewable generation, the proposed method only requires partial information of the underlying probability distribution. In addition, the mechanical voltage regulation devices and the DG inverters are controlled in two stages, considering their different characteristics in voltage control. By taking into account both the current and forecasted renewable generation, the proposed method utilizes receding horizon control to determine the control actions of voltage regulation devices. The effectiveness of the proposed method is demonstrated by case studies on unbalanced IEEE-123 bus system.

1. Introduction

Nowadays, driven by the concern on depletion of fossil fuels and environment protection, the renewable energy is playing an important role in today's energy pattern [1]. Integrating renewable-based distributed generations (DGs), such as residential wind turbines or rooftop photovoltaic panels, into distribution networks (DNs) is the common way to utilize the renewables [2]. However, the proliferation of renewable-based DGs brings severe operation challenges to DNs, with voltage control being one of them [3,4].

The main purpose of voltage/var control (VVC) in distribution networks (DNs) is to maintain the feeder voltages within allowed limits. Conventionally, DN voltages are regulated by utility-owned mechanical voltage control equipments, such as transformers with on-load tap changer (OLTC), step voltage regulators (SVRs) and switchable capacitor banks (CBs). However, the renewable generation is highly stochastic and uncertain in nature, leading to increased variability of feeder voltages that mechanical VVC devices may fail to handle [3]. Besides, regulating voltages under high-penetrated renewable scenario requires more frequent switching operation, which reduces the lifespan of these mechanical devices. On the other hand, DGs are integrated into DNs via fast-responding power electronics inverters. Thus, utilizing DG inverters for voltage control is a promising solution for above issue. The recent amended IEEE 1547 standard has allowed DGs to provide voltage regulation capabilities [5].

In general, determining the optimal setpoints of VVC devices under uncertainty is an instance of optimal power flow (OPF) tasks. Up to now, various technical approaches have been explored to tackle this problem, including stochastic programming (SP), robust optimization (RO) and chance-constrained programming (CC). In SP, the uncertain parameters are assumed to follow certain probability distribution (PD) and described using a finite number of scenarios. The authors in [6] proposed a multi-objective voltage control framework for DNs where the uncertainties associated with renewable generation are modeled by scenario methods. In [7], the uncertainty forecasting errors of generation and load were assumed to follow Beta distribution and normal distribution respectively. Similarly, voltage control problem was formulated as a two-stage SP in [8] where mechanical VVC devices and DG inverters were controlled in different timescales. However, scenario-based SP is criticized to be computational demanding [9]. In

☆ This work is supported by China Scholarship Council and Department of Energy Technology, Aalborg University.
* Corresponding author.
E-mail address: zhf@energy.aau.dk (Z. Zhang).

https://doi.org/10.1016/j.renene.2022.08.086
Received 30 May 2022; Received in revised form 4 August 2022; Accepted 18 August 2022
Available online 23 August 2022

Nomenclature

Abbreviations

CB	Capacitor banks
CC	Chance-constrained programming
DG	Distributed generation
DN	Distribution network
DRCC	Distributionally robust chance-constrained optimization
LSC	Lower stage controller
OLTC	On-load tap changer
OPF	Optimal power flow
PD	Probability distribution
RHC	Receding horizon control
RO	Robust optimization
SP	Stochastic programming
SVR	Step voltage regulator
TDRC-RHC	Two-stage distributionally robust chance-constrained receding horizon voltage control
USC	Upper stage controller
VVC	Voltage/var control

Parameters

β	Confidence parameter
δ_{tap}, δ_{c}	Constant difference between two consecutive tap position of OLTC/CB
ϵ	Allowed violation probability
ω_{mec}, ω_{p}	Weighting factors for mechanical VVC devices operation/power losses
$\overline{n}_{\text{c}}$, $\underline{n}_{\text{c}}$	Max/min CB tap position
$\overline{n}_{\text{tap}}$, $\underline{n}_{\text{tap}}$	Max/min OLTC tap position
$\overline{q}_{\text{inv}}$, $\underline{q}_{\text{inv}}$	Max/min DG inverter reactive power output
$\overline{u}$, $\underline{u}$	Upper/lower limit of voltage magnitude
$\Delta\overline{n}_{\text{c}}$, $\Delta\underline{n}_{\text{c}}$	Max/min ramping limit of CB tap position
$\Delta\overline{n}_{\text{tap}}$, $\Delta\underline{n}_{\text{tap}}$	Max/min ramping limit of OLTC tap position
Δq_{c}	CB reactive power output per step
c_{tap}, c_{c}, c_{p}	Cost coefficients of OLTC and CB operation, power losses
M	Big number in big-M method
N_k	Number of LSC control steps in T_c
N_p	Prediction step
N_{PV}	Dimension of uncertainties
S_{inv}	Capability of DG inverter
T_c, t_c	Control period of upper/lower stage controller
u_{nom}	Squared nominal voltage value

Sets

D	Ambiguity set
$\mathcal{L}$	Set of branches
$\mathcal{N}$	Set of buses

Variables

p_{inv}, q_{inv}	DG inverter real/reactive power output
p_{l}, q_{l}	Real/reactive power load consumption
q_{c}	CB reactive power output
$\overline{p}_{\text{inv}}$	Forecasted real power output of DG inverter
ξ	Uncertainty forecasting error
n_{tap}, n_{c}	Tap position of OLTC/CB
p, q	Real/reactive power injection
P_{loss}	Power losses
u	Squared voltage magnitude
z	Binary variable

addition, the actual PD of uncertainty variables may deviate from the pre-assumption or even hard to obtain in practice [10].

RO treats the uncertainty variables with an interval uncertainty set, and the optimal solution can be found under the worst-case scenario. In [11], a two-stage robust model was presented to dispatch real/reactive power in active DNs under wind power uncertainty. Multi-objective robust voltage control models were reported to minimize power losses in [12] and ensure the maximum renewable power capture in [13]. Even though RO is a computationally efficient alternative to SP, it often leads to over-conservative solutions [14].

Instead, the uncertainty constraints are guaranteed to be satisfied above a specific probability level in CC. The difficulty in CC is that the probability constraints cannot be solved straightforward. The common way is to use scenario method by evaluating a large number of random scenarios. For example, a CC-OPF was formulated in [15], wherein the forecasting errors are assumed to follow normal distribution. A two-stage chance-constrained approach was presented in [16] to address voltage control problem under uncertainty. But the method in [16] assumes that the uncertainties follow a specific probability distribution and the scenario method used to evaluate the chance constraints are not computational efficient. There are also other attempts to derive tractable approximation of original CC problem, e.g., the work in [17] established the linear expressions of chance constraint based on steady-state security region, [18] used affine disturbance parameterization to reformulate chance constraint into a second-order cone program to rendering the problem solvable. However, the methods in [17,18] are only valid if the underlying PD is normally distributed, which narrows their application in practice.

The previous CC voltage control approaches are either computational expensive or relying on strong assumptions that may not hold in practice. To address this issue, we propose a two-stage distributionally robust chance-constrained receding horizon voltage control algorithm (TDRC-RHC) in this paper, which is not only computational efficient but also relying on reasonable assumption of the uncertainties. Compared with the existing works in the area of DN voltage control, the advantages of proposed method are summarized as follows:

- The distributionally robust chance-constrained (DRCC) reformulation of CC voltage control in DNs is derived, in which the uncertainties of renewable generation are represented by an ambiguity set only require partial information of the underlying PD.
- Compared with the commonly used scenario method, the DRCC reformulation is exact and computationally efficient.
- The mechanical VVC devices and DG inverters with different voltage control characteristics are controlled in two stages. The control actions are determined using the idea of receding horizon control (RHC) by comprehensively considering the current and forecasted renewable generation.
- The performance of the proposed method is validated by case studies on unbalanced DNs.

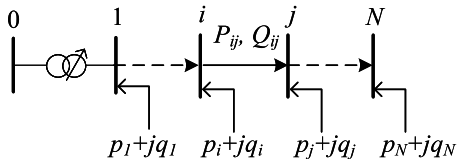

Fig. 1. Topology of a typical radial DN.

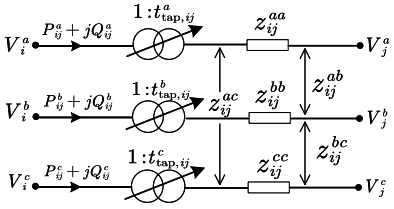

Fig. 2. Branch model with on-load tap changer.

The remainder of this paper is organized as follows[1]: Section 2 introduces modeling of unbalanced DNs. Section 3 formulates of the proposed TDRC-RHC voltage control algorithm. Case studies are presented in Section 4, followed by conclusions in Section 5.

2. Preliminaries

2.1. Multi-phase unbalanced DN model

As shown in Fig. 1, the topology of a typical radial DN is represented by $\mathcal{G} = (\mathcal{N}, \mathcal{L})$, where $\mathcal{N} := \{1, \ldots, N\}$ denotes set of buses while $\mathcal{L}$ denotes set of branches. Bus indexed by 0 denotes the substation bus and is assumed to be the reference bus. Without loss of generality, each bus or branch is assumed to have all three phases, yet represented by a 3×1 complex vector. For each bus $i \in \mathcal{N}$, let $\widetilde{V}_i := \left[V_i^a \; V_i^b \; V_i^c\right]^\top$ denote the three-phase voltages. For each branch $(i,j) \in \mathcal{L}$, let $\widetilde{I}_{ij} := \left[I_{ij}^a \; I_{ij}^b \; I_{ij}^c\right]^\top$ and $\widetilde{S}_{ij} := \left[S_{ij}^a \; S_{ij}^b \; S_{ij}^c\right]^\top$ denote its three-phase line current and complex power flow, respectively.

As shown in Fig. 2, the three-phase power flow equation for each branch including OLTC tap ratio $\widetilde{t}_{\mathrm{tap},ij}$ is governed by Ohm's law,

$$\widetilde{S}_{ij} - \mathrm{diag}\left(\widetilde{z}_{ij}\widetilde{I}_{ij}\right)\widetilde{I}_{ij}^* - \sum_{k\in\mathcal{N}_j}\widetilde{S}_{jk} = -\widetilde{s}_j \tag{1a}$$

$$\widetilde{t}_{\mathrm{tap},ij} \odot \widetilde{V}_i - \widetilde{z}_{ij}\widetilde{I}_{ij} = \widetilde{V}_j \tag{1b}$$

where $\widetilde{z}_{ij} := \widetilde{r}_{ij} + j\widetilde{x}_{ij} \in \mathbb{C}^{3\times 3}$ is 3×3 full symmetric impedance matrix of branch (i,j) and $\widetilde{t}_{\mathrm{tap},ij} = 1 + \widetilde{n}_{\mathrm{tap},ij}\Delta tap_{ij}$ with $\widetilde{n}_{\mathrm{tap},ij}$ is three-phase OLTC tap position and Δtap_{ij} is OLTC voltage change per step.

To eliminate voltage angles, both sides in (1b) are multiplied by their complex conjugates,

$$\widetilde{t}^2_{\mathrm{tap},ij} \odot \widetilde{u}_i - 2\mathrm{Re}\left[\widetilde{V}_i \odot \left(\widetilde{z}_{ij}^* \widetilde{I}_{ij}^*\right)\right] + \left(\widetilde{z}_{ij}\widetilde{I}_{ij}\right) \odot \left(\widetilde{z}_{ij}^* \widetilde{I}_{ij}^*\right) = \widetilde{u}_j \tag{2}$$

where $\widetilde{u}_i := \left[\left|V_i^a\right|^2 \; \left|V_i^b\right|^2 \; \left|V_i^c\right|^2\right]^\top$ represents the three-phase squared voltage magnitude at bus i.

[1] Boldface letters denote matrix or column vectors, $\widetilde{(\cdot)}$ represents three-phase variables, $(\cdot)^\top$ for transposition, $(\cdot)^*$ is complex conjugate and $(\cdot)^{\mathrm{H}}$ is complex conjugate transposition, $\otimes$ denotes Kronecker product, $\odot$ element-wise multiplication. $\mathfrak{R}(\cdot)$ and $\mathfrak{I}(\cdot)$ represent the real/imaginary part of a complex variable. $\boldsymbol{I}_N$ denotes the $N \times N$ identity matrix. For variable $\boldsymbol{x}$, $\|\boldsymbol{x}\|_2$ is its 2-norm while $\mathrm{diag}(\boldsymbol{x})$ returns a $N \times N$ matrix with $\boldsymbol{x}$ in its diagonal. The abbreviations and notations are summarized in nomenclature and some of them are explained the first time they appear.

Given the fact that voltage magnitudes between phases are similar, we have $\widetilde{V}_i \approx |V_i|\,\boldsymbol{\alpha}$, $\boldsymbol{\alpha} := \left[1 \; \alpha \; \alpha^2\right]^\top$, $\alpha = e^{-j(2\pi/3)}$. Also last term in (2) is rather small and negligible, (2) can be approximated as [19],

$$\widetilde{t}^2_{\mathrm{tap},ij} \odot \widetilde{u}_i - \widetilde{u}_j = 2\mathrm{Re}\left[\mathrm{diag}\left(\boldsymbol{\alpha}^*\right)\widetilde{z}_{ij}^* \mathrm{diag}\left(\boldsymbol{\alpha}\right)\widetilde{S}_{ij}\right] \tag{3}$$

Eq. (3) can be equivalent given as,

$$\widetilde{t}^2_{\mathrm{tap},ij} \odot \widetilde{u}_i - \widetilde{u}_j = 2\left(\hat{r}_{ij}\widetilde{P}_{ij} + \hat{x}_{ij}\widetilde{Q}_{ij}\right) \tag{4}$$

where

$$\hat{r}_{ij} = \mathfrak{R}\left(\boldsymbol{\alpha}\boldsymbol{\alpha}^{\mathrm{H}}\right) \odot \widetilde{r}_{ij} + \mathfrak{I}\left(\boldsymbol{\alpha}\boldsymbol{\alpha}^{\mathrm{H}}\right) \odot \widetilde{x}_{ij}$$
$$\hat{x}_{ij} = \mathfrak{R}\left(\boldsymbol{\alpha}\boldsymbol{\alpha}^{\mathrm{H}}\right) \odot \widetilde{x}_{ij} - \mathfrak{I}\left(\boldsymbol{\alpha}\boldsymbol{\alpha}^{\mathrm{H}}\right) \odot \widetilde{r}_{ij}$$

The term $\widetilde{t}^2_{\mathrm{tap},ij}\widetilde{u}_i$ makes the problem nonconvex, it can be linearized as [20],

$$\begin{aligned}\widetilde{t}^2_{\mathrm{tap},ij} \odot \widetilde{u}_i &= \left(1 + 2\widetilde{n}_{\mathrm{tap},ij} \cdot \Delta tap_{ij} + \widetilde{n}^2_{\mathrm{tap},ij} \cdot \left(\Delta tap_{ij}\right)^2\right) \odot \widetilde{u}_i \\ &\approx \widetilde{u}_i + 2\widetilde{n}_{\mathrm{tap},ij} \cdot \Delta tap_{ij} \odot \widetilde{u}_i \\ &\approx \widetilde{u}_i + 2\widetilde{n}_{\mathrm{tap},ij} \cdot \Delta tap_{ij} \cdot u_{\mathrm{nom}}\end{aligned} \tag{5}$$

where u_{nom} is the squared nominal voltage value.

Such approximation holds as $\widetilde{n}^2_{\mathrm{tap},ij} \cdot \left(\Delta tap_{ij}\right)^2 \approx 0$ and bus voltages are around the reference during normal operation. Thus, the linear approximation of multi-phase branch flow model is expressed as,

$$\widetilde{P}_{ij} - \sum_{k\in\mathcal{N}_j}\widetilde{P}_{jk} = -\widetilde{p}_j \tag{6a}$$

$$\widetilde{Q}_{ij} - \sum_{k\in\mathcal{N}_j}\widetilde{Q}_{jk} = -\widetilde{q}_j \tag{6b}$$

$$\widetilde{u}_i - \widetilde{u}_j = 2\left(\hat{r}_{ij}\widetilde{P}_{ij} + \hat{x}_{ij}\widetilde{Q}_{ij}\right) - 2\widetilde{n}_{\mathrm{tap},ij}\Delta tap_{ij}u_{\mathrm{nom}} \tag{6c}$$

2.2. Compact form representation of multi-phase DN model

For notational brevity, we introduce a matrix form representation of multi-phase DN model in this section. Firstly, squared voltage magnitudes, real/reactive power injection in set $\mathcal{N}$ are collected into column vectors $\boldsymbol{u} := \left[\widetilde{u}_1^\top \cdots \widetilde{u}_N^\top\right]^\top$, $\boldsymbol{p} := \left[\widetilde{p}_1^\top \cdots \widetilde{p}_N^\top\right]^\top$ and $\boldsymbol{q} := \left[\widetilde{q}_1^\top \cdots \widetilde{q}_N^\top\right]^\top \in \mathbb{R}^{3N}$, respectively. Similarly, branch real/reactive power flow in set $\mathcal{L}$ and tap positions of OLTC and CBs are collected into column vector $\boldsymbol{P}$, $\boldsymbol{Q}$, $\boldsymbol{n}_{\mathrm{tap}}$ and $\boldsymbol{n}_{\mathrm{c}}$, respectively. Then, let $\bar{\boldsymbol{G}} := \left[\boldsymbol{g}_0 \; \boldsymbol{G}^\top\right]^\top \in \{0, \pm 1\}^{(N+1)\times N}$ denote the incidence matrix of $\mathcal{G}$, which is defined as: $\bar{\boldsymbol{G}}_{il} = 1$ if branch l starts at bus i whereas $\bar{\boldsymbol{G}}_{il} = -1$ if branch l ends at bus i, otherwise $\bar{\boldsymbol{G}}_{il} = 0$ [21]. $\boldsymbol{g}_0^\top$ is the first row of $\bar{\boldsymbol{G}}$ and $\boldsymbol{G}$ is the remaining submatrix. Define block diagonal matrix $\hat{\boldsymbol{R}} := \mathrm{diag}\left(\left\{\hat{R}_\ell\right\}\right) \in \mathbb{R}^{3N\times 3N}$ with ℓ_th diagonal element equals to $\hat{\boldsymbol{r}}_{ij}$ of the ℓ_th branch $\in \mathcal{L}$, the same is with $\hat{\boldsymbol{X}} := \mathrm{diag}\left(\left\{\hat{X}_\ell\right\}\right) \in \mathbb{R}^{3N\times 3N}$. Extending the incidence matrix of $\mathcal{G}$ into three phases by

$$\bar{\boldsymbol{A}} := \bar{\boldsymbol{G}} \otimes \boldsymbol{I}_3 \tag{7}$$

The compact form of (6a)–(6c) can be represented by

$$-\boldsymbol{A}\boldsymbol{P} = -\boldsymbol{p} \tag{8a}$$

$$-\boldsymbol{A}\boldsymbol{Q} = -\boldsymbol{q} \tag{8b}$$

$$\left[\boldsymbol{a}_0 \; \boldsymbol{A}^\top\right]\begin{bmatrix}\boldsymbol{u}_0 \\ \boldsymbol{u}\end{bmatrix} = 2\left(\hat{\boldsymbol{R}}\boldsymbol{P} + \hat{\boldsymbol{X}}\boldsymbol{Q}\right) - 2u_{\mathrm{nom}}\boldsymbol{n}_{\mathrm{tap}} \odot \Delta\boldsymbol{tap} \tag{8c}$$

Substituting (8a) and (8b) into (8c) to obtain,

$$\boldsymbol{u} = 2\left(\boldsymbol{D}_r\boldsymbol{p} + \boldsymbol{D}_x\boldsymbol{q}\right) - 2u_{\mathrm{nom}}\boldsymbol{n}_{\mathrm{tap}} \odot \Delta\boldsymbol{tap} - \boldsymbol{A}^{-\top}\boldsymbol{a}_0\boldsymbol{u}_0 \tag{9}$$

where $\boldsymbol{D}_r := \boldsymbol{A}^{-\top}\hat{\boldsymbol{R}}\boldsymbol{A}^{-1}$ and $\boldsymbol{D}_x = \boldsymbol{A}^{-\top}\hat{\boldsymbol{X}}\boldsymbol{A}^{-1}$

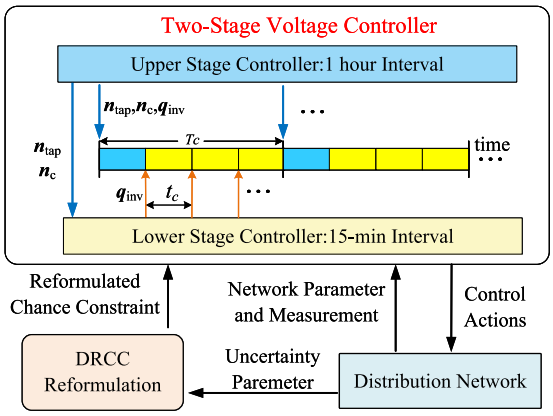

Fig. 3. Schematic diagram of the proposed TDRC-RHC.

3. Formulation of the proposed algorithm

In this section, we introduce the details of the proposed TDRC-RHC voltage control algorithm. The diagram of the proposed algorithm is illustrated in Fig. 3. As shown in Fig. 3, there are mainly two parts in the proposed algorithm, the two-stage voltage controller based on RHC and the DRCC reformulation of chance constraint.

3.1. Two-stage voltage controller

The response speed of mechanical VVC devices is usually ranging from several seconds to minutes, which is not fast enough to accommodate the voltage variation caused by fluctuation of renewable generation [8]. In addition, the frequent switching operation could dramatically reduce their lifetime. On the other hand, the fast-response DG inverters(response speed in millisecond) can provide reactive power to support feeder voltages. Considering the different characteristics of VVC devices, the proposed algorithm is decomposed into two stages. The slow-response mechanical VVC equipments, OLTC transformer and CBs, are controlled in the upper stage with a longer control period T_c of 1 h to regulate the overall voltage profile whereas the reactive power outputs of fast-response DG inverters are dispatched in the lower stage with a shorter control period t_c of 15-min in response to fast voltage variations. The control period of upper stage and lower stage are chosen based on the time period of SCADA system and advanced metering infrastructure (AMI) in some real practices [22,23], as well as recommendations from relevant guideline and literature [8,24]. In the whole control period, DG inverters keep operating at maximum power point tracking (MPPT) mode to capture maximum active power [25,26].

3.1.1. Upper stage controller

The main purpose of upper stage controller(USC) is to maintain the bus voltages in the allowed range and to reduce the number of operation of mechanical VVC devices to prolong their lifetime. Also, adjusting the DG inverter reactive power outputs has strong impact on network power losses [27], so power losses minimize are also considered in USC. When determining the control actions of VVC devices, the idea of RHC is used to improve the algorithm performance by taking into account not only the current renewable generation, but also its predicted value over a chosen future time horizon. Thus, the mathematical formulation of USC at time instant t is given as,

$$\min_{\boldsymbol{n}_{\text{tap}},\boldsymbol{n}_{\text{c}},\boldsymbol{q}_{\text{inv}}} \sum_{k=t}^{t+N_p-1} \begin{bmatrix} \omega_{\text{mec}}\left(c_{\text{tap}}\|\boldsymbol{n}_{\text{tap}}(k)-\boldsymbol{n}_{\text{tap}}(k-1)\|_2 \right. \\ \left. + c_{\text{c}}\|\boldsymbol{n}_{\text{c}}(k)-\boldsymbol{n}_{\text{c}}(k-1)\|_2\right) \\ +\omega_{\text{p}} \sum_{i=t}^{t+N_k-1} c_{\text{p}} P_{\text{loss}}(i) \end{bmatrix} \tag{10a}$$

subject to,

$$\boldsymbol{u}(k) = 2\left(\boldsymbol{D}_r\boldsymbol{p}(k) + \boldsymbol{D}_x\boldsymbol{q}(k)\right) - 2u_{\text{nom}}\boldsymbol{n}_{\text{tap}}(k) \odot \Delta\boldsymbol{tap} - \boldsymbol{A}^{-\top}\boldsymbol{a}_0\boldsymbol{u}_0 \tag{10b}$$

$$\boldsymbol{p}(k) = \boldsymbol{p}_{\text{inv}}(k) - \boldsymbol{p}_{\text{l}}(k) \tag{10c}$$

$$\boldsymbol{q}(k) = \boldsymbol{q}_{\text{inv}}(k) + \boldsymbol{q}_{\text{c}}(k) - \boldsymbol{q}_{\text{l}}(k) \tag{10d}$$

$$\boldsymbol{p}_{\text{inv}}(k) = \overline{\boldsymbol{p}}_{\text{inv}}(k) + \boldsymbol{\xi}(k) \tag{10e}$$

$$\underline{\boldsymbol{q}}_{\text{inv}}(k) \leqslant \boldsymbol{q}_{\text{inv}}(k) \leqslant \overline{\boldsymbol{q}}_{\text{inv}}(k) \tag{10f}$$

$$-\underline{\boldsymbol{q}}_{\text{inv}}(k) = \overline{\boldsymbol{q}}_{\text{inv}}(k) = \sqrt{\boldsymbol{S}_{\text{inv}}^2 - \left(\boldsymbol{p}_{\text{inv}}(k)\right)^2} \tag{10g}$$

$$P_{\text{loss}}(k) = \sum_{(i,j)\in\mathcal{L},\phi\in\{a,b,c\}} \hat{r}_{ij}^{\phi} \frac{\left(P_{ij}^{\phi}(k)\right)^2 + \left(Q_{ij}^{\phi}(k)\right)^2}{u_{\text{nom}}} \tag{10h}$$

$$\mathbb{P}\left(\underline{\boldsymbol{u}} \leqslant \boldsymbol{u}(k) \leqslant \overline{\boldsymbol{u}}\right) \geqslant 1-\epsilon \tag{10i}$$

$$\underline{\boldsymbol{n}}_{\text{tap}} \leqslant \boldsymbol{n}_{\text{tap}}(k) \leqslant \overline{\boldsymbol{n}}_{\text{tap}} \tag{10j}$$

$$\Delta\underline{\boldsymbol{n}}_{\text{tap}} \leqslant \boldsymbol{n}_{\text{tap}}(k) - \boldsymbol{n}_{\text{tap}}(k-1) \leqslant \Delta\overline{\boldsymbol{n}}_{\text{tap}} \tag{10k}$$

$$\boldsymbol{q}_{\text{c}}(k) = \boldsymbol{n}_{\text{c}}(k) \cdot \Delta q_{\text{c}} \tag{10l}$$

$$\underline{\boldsymbol{n}}_{\text{c}} \leqslant \boldsymbol{n}_{\text{c}}(k) \leqslant \overline{\boldsymbol{n}}_{\text{c}} \tag{10m}$$

$$\Delta\underline{n}_{\text{c}} \leqslant \boldsymbol{n}_{\text{c}}(k) - \boldsymbol{n}_{\text{c}}(k-1) \leqslant \Delta\overline{n}_{\text{c}} \tag{10n}$$

$$N_k = T_c/t_c \tag{10o}$$

where (10b)–(10i) is the power flow constraints with (10i) representing the CC voltage constraint, ϵ is the allowed violation probability. (10j)–(10k) and (10l)–(10n) are operation constraints for OLTC transformer and CB, respectively. (10f)–(10g) are DG inverter operation constraints. N_p is the prediction step. c_{tap}, c_{c} and c_{p} are cost coefficients for OLTC, CB operation and power losses. ω_{mec} and ω_{p} are weighting factors for mechanical VVC equipments operation and power losses, respectively. The weighting factors can be determined by analytical hierarchy process method according to the preference of decision makers [28].

The bilinear terms in (10b) and (10l) can be linearized by big-M method [16],

$$n_{\text{tap}} = \underline{n}_{\text{tap}} + \delta_{\text{tap}} \sum_{k=0}^{m_{\text{tap}}} 2^k z_{\text{tap}},\ z_{\text{tap}} \in \{0,1\} \tag{11a}$$

$$\underline{n}_{\text{tap}} + \delta_{\text{tap}} \sum_{k=0}^{m_{\text{tap}}} 2^k z_{\text{tap}} \leqslant \overline{n}_{\text{tap}} \tag{11b}$$

$$c = \Delta tap u_{\text{nom}},\ w_{\text{tap}} = z_{\text{tap}} c \tag{11c}$$

$$c - M\left(1-z_{\text{tap}}\right) \leqslant w_{\text{tap}} \leqslant c + M\left(1-z_{\text{tap}}\right) \tag{11d}$$

$$-M z_{\text{tap}} \leqslant w_{\text{tap}} \leqslant M z_{\text{tap}} \tag{11e}$$

$$n_{\text{c}} = \underline{n}_{\text{c}} + \delta_{\text{c}} \sum_{k=0}^{m_{\text{c}}} 2^k z_{\text{c}},\ z_{\text{c}} \in \{0,1\} \tag{11f}$$

$$\underline{n}_{\text{c}} + \delta_{\text{c}} \sum_{k=0}^{m_{\text{c}}} 2^k z_{\text{c}} \leqslant \overline{n}_{\text{c}} \tag{11g}$$

$$w_{\text{c}} = z_{\text{c}} \Delta q_{\text{c}} \tag{11h}$$

$$\Delta q_{\text{c}} - M\left(1-z_{\text{c}}\right) \leqslant w_{\text{c}} \leqslant \Delta q_{\text{c}} + M\left(1-z_{\text{c}}\right) \tag{11i}$$

$$-M z_{\text{c}} \leqslant w_{\text{c}} \leqslant M z_{\text{c}} \tag{11j}$$

The USC is optimized at the beginning of an hour, the input is the network real/reactive load consumption $\boldsymbol{p}_{\text{l}}(k)$ and $\boldsymbol{q}_{\text{l}}(k)$, the forecasting renewable generation $\overline{\boldsymbol{p}}_{\text{inv}}(k)$ and the uncertainty forecasting errors $\boldsymbol{\xi}(t)$ for the future N_p steps. The output of USC is the tap positions of OLTC transformer $\boldsymbol{n}_{tap}(T_c)$ and CBs $\boldsymbol{n}_c(T_c)$ for the whole hour, as well as the DG inverters reactive power outputs $\boldsymbol{q}_{\text{inv}}(t_c)$ for the first 15 min of an hour.

3.1.2. Lower stage controller

The lower stage controller(LSC) receives tap positions of mechanical VVC devices from USC, then determines the DG inverters reactive

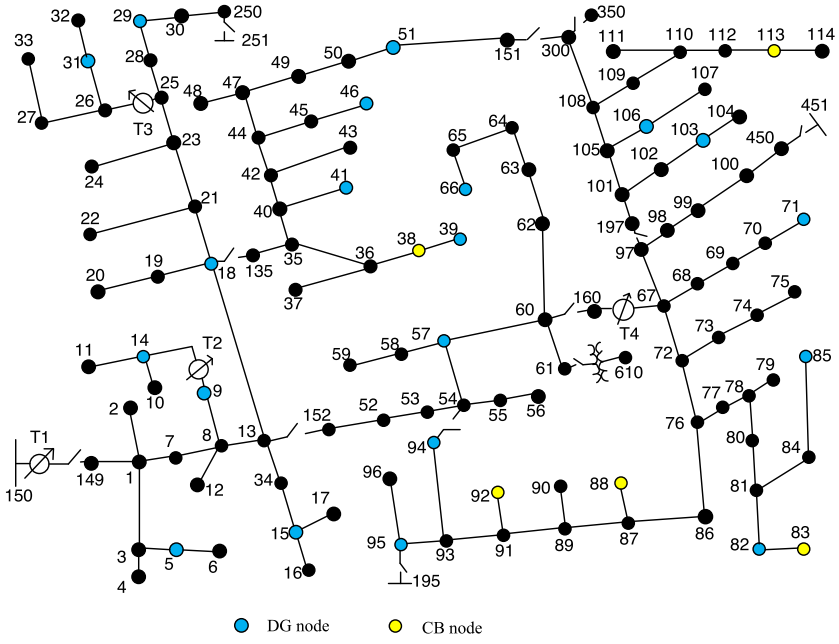

Fig. 4. IEEE-123 bus test feeder.

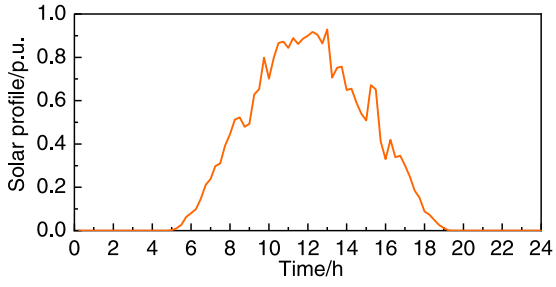

Fig. 5. Solar profile.

power dispatch for the rest 45-min of an hour. The main objective of LSC is to minimize the network power losses and regulate the bus voltages in the allowed limits by dispatching the reactive power outputs of DG inverters. So the optimization problem of LSC at time t is formulated as,

$$\min_{\boldsymbol{q}_{\text{inv}}} P_{\text{loss}}(t) \tag{12a}$$

subject to

$$\boldsymbol{u}(t) = 2\left(\boldsymbol{D}_r \boldsymbol{p}(t) + \boldsymbol{D}_x \boldsymbol{q}(t)\right) - 2u_{\text{nom}} \boldsymbol{n}_{\text{tap}}\left(T_{\text{c}}\right) \odot \Delta \boldsymbol{tap} - \boldsymbol{A}^{-\top} \boldsymbol{a}_0 \boldsymbol{u}_0 \tag{12b}$$

$$\boldsymbol{p}(t) = \boldsymbol{p}_{\text{inv}}(t) - \boldsymbol{p}_{\text{l}}(t) \tag{12c}$$

$$\boldsymbol{q}(t) = \boldsymbol{q}_{\text{inv}}(t) + \boldsymbol{q}_{\text{c}}\left(T_{\text{c}}\right) - \boldsymbol{q}_{\text{l}}(t) \tag{12d}$$

$$\boldsymbol{p}_{\text{inv}}(t) = \overline{\boldsymbol{p}}_{\text{inv}}(t) + \boldsymbol{\xi}(t) \tag{12e}$$

$$\underline{\boldsymbol{q}}_{\text{inv}}(t) \leqslant \boldsymbol{q}_{\text{inv}}(t) \leqslant \overline{\boldsymbol{q}}_{\text{inv}}(\text{t}) \tag{12f}$$

$$-\underline{\boldsymbol{q}}_{\text{inv}}(t) = \overline{\boldsymbol{q}}_{\text{inv}}(t) = \sqrt{\boldsymbol{S}_{\text{inv}}^2 - \left(\boldsymbol{p}_{\text{inv}}(t)\right)^2} \tag{12g}$$

$$P_{\text{loss}}(t) = \sum_{(i,j)\in\mathcal{L},\phi\in\{a,b,c\}} \hat{r}_{ij}^{\phi} \frac{\left(P_{ij}^{\phi}(t)\right)^2 + \left(Q_{ij}^{\phi}(t)\right)^2}{u_{\text{nom}}} \tag{12h}$$

$$\mathbb{P}\left(\underline{\boldsymbol{u}} \leqslant \boldsymbol{u}(t) \leqslant \overline{\boldsymbol{u}}\right) \geqslant 1 - \epsilon \tag{12i}$$

The input of LSC is the network real/reactive load consumption $\boldsymbol{p}_{\text{l}}(t)$ and $\boldsymbol{q}_{\text{l}}(t)$, the tap positions of OLTC transformer $\boldsymbol{n}_{\text{tap}}\left(T_c\right)$ and CBs $\boldsymbol{n}_{\text{c}}\left(T_c\right)$ from USC as well as the forecasting renewable generation $\overline{\boldsymbol{p}}_{\text{inv}}(t)$ and the uncertainty forecasting errors $\boldsymbol{\xi}(t)$. The output of LSC is DG inverters reactive power outputs $\boldsymbol{q}_{\text{inv}}\left(t_{\text{c}}\right)$ for the current 15-min control period.

3.2. Chance constraint scenario method

The probability constraint in (10i) cannot be solved directly. The commonly used way in previous studies is to transform the probability constraint into hard constraint via scenario method. The authors in [29] proved that if the number of randomly generated samples of the uncertain parameters is above a lower bound, then the resulted solution is exact for the original CC problem with a certain confidence level. For mixed integer problem whose continuous relaxation is convex and integer variable lies in the set $\{0,1\}$, the number of samples needs to generate is given as [16],

$$2^l \sum_{i=0}^{n-1} \binom{N}{i} \epsilon^i (1-\epsilon)^{N-i} \leqslant \beta \tag{13}$$

where n is the number of continuous variable and l is the number of binary variables. $\beta \in (0,1)$ is the confidence parameter describing the original chance constraint can be guaranteed with confidence level at least $1-\beta$.

3.3. DRCC reformulation of chance constraint

The scenario method is known to be computational demanding, especially for increasing number of uncertain variables. In addition, the true PD of uncertainty variables may deviate from the assumed one or such PD may not even be accessible in reality. To overcome this issue, we introduce the DRCC reformulation of the original chance-constrained problem in this section, which is not only accurate but also computational efficient. Rather than assumption of perfect knowledge of the PD, the forecasting errors of renewable generation are represented by an ambiguity set which requires only the first-order and second-order moments in our method. The moment-based ambiguity set D defined with mean(first-order moment) and covariance matrix (second-order moment) is given as [30],

$$D = \left\{\mathbb{P} \in \left(\mathbb{R}^{N_{\text{PV}}}\right), \mathbb{E}_{\mathbb{P}}(\boldsymbol{\xi}) = 0, \mathbb{E}_{\mathbb{P}}\left(\boldsymbol{\xi}\boldsymbol{\xi}^{\top}\right) = \boldsymbol{\Sigma}\right\} \tag{14}$$

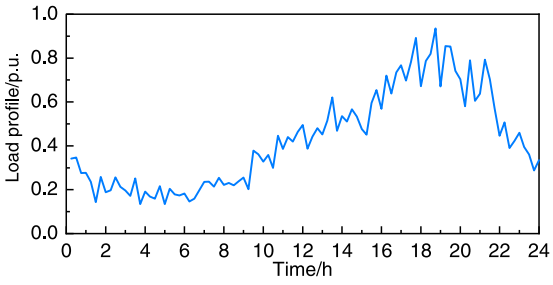

Fig. 6. Load profile.

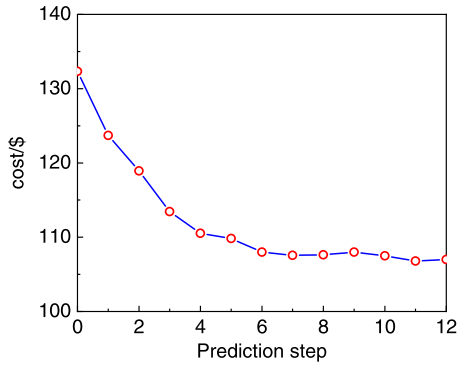

Fig. 7. Performance with different prediction steps.

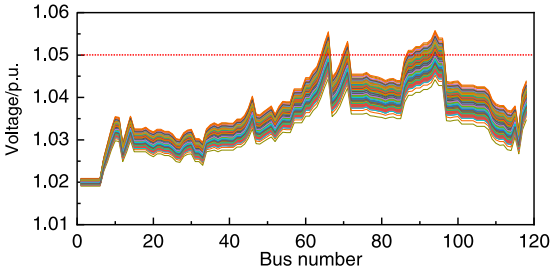

Fig. 8. Voltage in deterministic optimization.

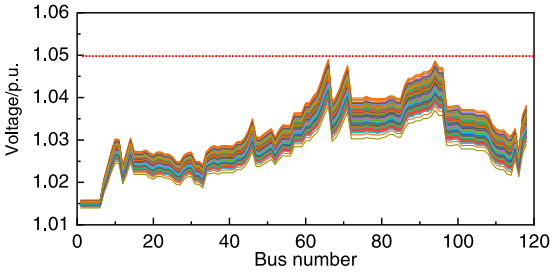

Fig. 9. Voltage in TDRC-RHC optimization.

where $\left(\mathbb{R}^{N_{\mathrm{PV}}}\right)$ denotes the set of all PDs on $\mathbb{R}^{N_{\mathrm{PV}}}$, N_{PV} is the dimension of $\boldsymbol{\xi}$. $\boldsymbol{\Sigma}$ is the semi-definite covariance matrix($\boldsymbol{\Sigma} \succeq 0$).

To start with, we recall Eq. (9) and applying it over two consecutive time instances, the voltage difference $\Delta \boldsymbol{u}(t) := \boldsymbol{u}(t) - \boldsymbol{u}(t-1)$ can be represented as,

$$\Delta \boldsymbol{u}(t) = 2\left(\boldsymbol{D}_r \Delta \boldsymbol{p}(t) + \boldsymbol{D}_x \Delta \boldsymbol{q}(t)\right) - 2u_{\mathrm{nom}} \Delta \boldsymbol{n}_{\mathrm{tap}}(t) \odot \Delta \boldsymbol{tap} \tag{15}$$

where vectors $\Delta \boldsymbol{p}(t)$, $\Delta \boldsymbol{q}(t)$ and $\Delta \boldsymbol{n}_{\mathrm{tap}}(t)$ are the difference of real/reactive power injection and OLTC tap positions between two time instances. From (15) we can see that $\boldsymbol{D}_r$ and $\boldsymbol{D}_x$ can be viewed as voltage sensitivity with respect to the network real/reactive power injections.

To derive the tractable reformulation of the original chance-constrained problem, we have the following assumptions:

(1) The forecasted renewable generation is accurate and the forecasting errors $\boldsymbol{\xi}$ are small. This assumption is reasonable as modern weather forecasting tools perform well in short-term forecasting [31].
(2) The real system operation status is close to the forecasted operation point($\boldsymbol{\xi} = 0$), the system forecasting operation point is denoted as $\boldsymbol{y}_0$.
(3) The impact of uncertainties on the network constraints can be modeled as the first order Taylor polynomial around the forecasting operation point, this assumption is reasonable considering the forecasting errors are sufficient small compared with the renewable generation.

Based on above assumptions, the bus voltages considering the uncertain forecasting errors can be represented as,

$$\boldsymbol{u} \approx \boldsymbol{u}_0 + (\partial \boldsymbol{u}/\partial \boldsymbol{\xi})\boldsymbol{\xi} \tag{16}$$

Clearly, the expectation and variance of $\boldsymbol{u}$ are $E(\boldsymbol{u}) = \boldsymbol{u}_0$ and $\mathrm{Var}(\boldsymbol{u}) = (\partial \boldsymbol{u}/\partial \boldsymbol{\xi})\,\mathrm{Var}(\boldsymbol{\xi})(\partial \boldsymbol{u}/\partial \boldsymbol{\xi})^{\top}$.

Define $\partial \boldsymbol{u}/\partial \boldsymbol{\xi} := \boldsymbol{\Gamma}$, from (10b) (10e) (15) we get,

$$\boldsymbol{\Gamma} = (\partial \boldsymbol{u}/\partial \boldsymbol{p})(\partial \boldsymbol{p}/\partial \boldsymbol{\xi}) \tag{17}$$

$$\partial \boldsymbol{u}/\partial \boldsymbol{p} = 2\boldsymbol{D}_r, \partial \boldsymbol{p}/\partial \boldsymbol{\xi} = \boldsymbol{I}_{N_{\mathrm{PV}}} \tag{18}$$

To obtain the DRCC reformulation of the original chance constraint, the upper bound voltage constraint $\mathbb{P}\left(\boldsymbol{u}_i \leqslant \overline{\boldsymbol{u}}\right) \geqslant 1-\epsilon$ is expressed by,

$$\Theta_D\left(\boldsymbol{u}_i \leqslant \overline{\boldsymbol{u}}\right) \geqslant 1-\epsilon \tag{19}$$

where $\Theta_D(\cdot)$ denotes the worst case cumulative distribution function in ambiguity set D.

Let $\mathbf{e}_i$ denote the ith column of the identity matrix, then the variance of $\boldsymbol{u}_i$ is given as $\left\|\mathbf{e}_i^{\top}\boldsymbol{\Gamma}\boldsymbol{\Sigma}^{1/2}\right\|_2$. Hence the DRCC reformulation of (19) is given as,

$$\left(\overline{\boldsymbol{u}} - \boldsymbol{u}_{0,i}\right) / \|\mathbf{e}_i^{\top}\boldsymbol{\Gamma}\boldsymbol{\Sigma}^{1/2}\|_2 \geqslant \Theta_D^{-1}(1-\epsilon) \tag{20}$$

where $\Theta_D^{-1}(1-\epsilon)$ is the inverse cumulative distribution function. For ambiguity set with known mean and covariance [32],

$$\Theta_D{}^{-1}(1-\epsilon) := \sqrt{(1-\epsilon)/\epsilon} \tag{21}$$

Substituting (21) into (20) to get,

$$\boldsymbol{u}_{0,i} \leqslant \overline{\boldsymbol{u}} - \sqrt{(1-\epsilon)/\epsilon}\|\mathbf{e}_i^{\top}\boldsymbol{\Gamma}\boldsymbol{\Sigma}^{1/2}\|_2 \tag{22}$$

Similarly, the lower bound voltage constraint $\mathbb{P}\left(\boldsymbol{u}_i \geqslant \underline{\boldsymbol{u}}\right) \geqslant 1-\epsilon$ can be also reformulated in the same way. Thus the DRCC reformulation of voltage constraint (10i) (12i) is given as,

$$\boldsymbol{u}_i \leqslant \overline{\boldsymbol{u}} - \lambda_i \tag{23a}$$

$$\boldsymbol{u}_i \geqslant \underline{\boldsymbol{u}} + \lambda_i \tag{23b}$$

$$\lambda_i = \sqrt{(1-\epsilon)/\epsilon}\|\mathbf{e}_i^{\top}\boldsymbol{\Gamma}\boldsymbol{\Sigma}^{1/2}\|_2 \tag{23c}$$

The term λ_i introduces a safety margin on the original voltage constraints against the uncertainty, λ_i increases with ϵ decreasing, which means that the safety margin will become larger when smaller violation probability is allowed. The inequality in (23a)–(23c) is deterministic in nature which is efficient to compute.

To better illustrate the proposed method, the overall process in TDRC-RHC is summarized in Algorithm 1

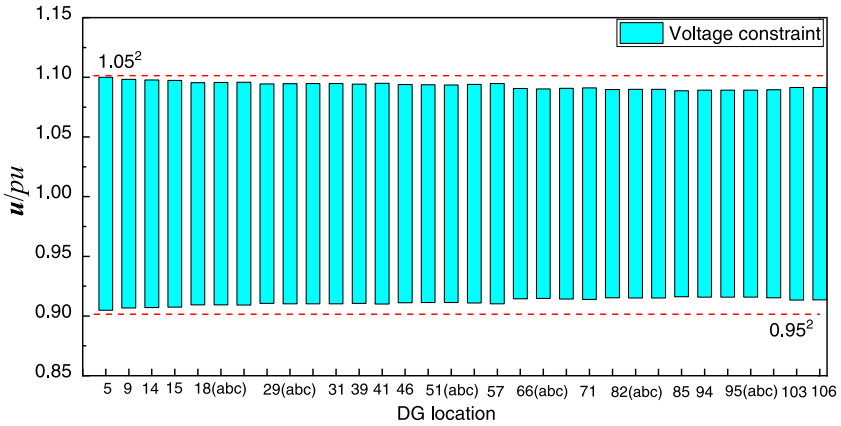

Fig. 10. Voltage constraint in TDRC-RHC.

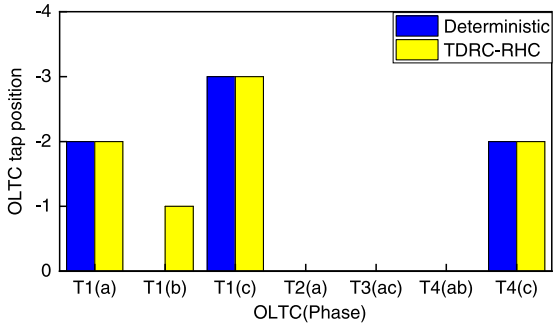

Fig. 11. OLTC tap positions.

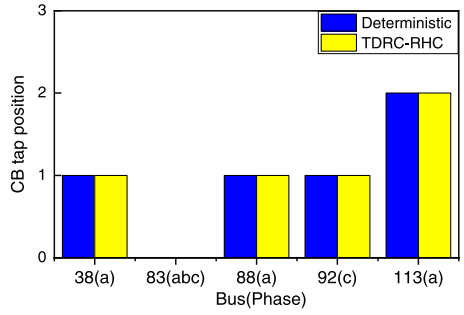

Fig. 12. CB tap positions.

Algorithm 1 The proposed TDRC-RHC

Require: Network parameters including incidence matrix $\overline{\boldsymbol{A}}$, block diagonal matrix $\hat{\boldsymbol{R}}$ and $\hat{\boldsymbol{X}}$. Real/reactive load consumption $\boldsymbol{p}_{\mathrm{l}}$ and $\boldsymbol{q}_{\mathrm{l}}$, forecasting renewable generation $\overline{\boldsymbol{p}}_{\mathrm{inv}}$, ambiguity set D of forecasting errors $\boldsymbol{\xi}$

for T_{c}=1,...,$T_{\mathrm{c,max}}$ **do**
  USC ← $\boldsymbol{p}_{\mathrm{l}}, \boldsymbol{q}_{\mathrm{l}}, \overline{\boldsymbol{p}}_{\mathrm{inv}}, \boldsymbol{\xi}$ for the future N_p steps
  Calculate $\boldsymbol{n}_{\mathrm{tap}}(T_c)$, $\boldsymbol{n}_{\mathrm{c}}(T_c)$ and $\boldsymbol{q}_{\mathrm{inv}}$ according to Eq. (10)(11)(23)
  Send $\boldsymbol{n}_{\mathrm{tap}}(T_c)$ and $\boldsymbol{n}_{\mathrm{c}}(T_c)$ to LSC
  for t_{c}=1,...,N_k **do**
    LSC ← $\boldsymbol{n}_{\mathrm{tap}}(T_c), \boldsymbol{n}_{\mathrm{c}}(T_c)$
    LSC ← $\boldsymbol{p}_{\mathrm{l}}, \boldsymbol{q}_{\mathrm{l}}, \overline{\boldsymbol{p}}_{\mathrm{inv}}, \boldsymbol{\xi}$
    Calculate $\boldsymbol{q}_{\mathrm{inv}}(t_{\mathrm{c}})$ according to Eq. (12)(23)
  end for
end for

4. Case study

4.1. System configuration

In this section, the performance of the proposed TDRC-RHC is verified on unbalanced IEEE-123 bus system, network parameters can be found in [33]. Simulations are developed in MATLAB r2020b with YALMIP Toolbox on an ordinary computer running Win10 with 3.9 GHz CPU and 32G RAM. The two-stage optimization problem is solved by Gurobi solver [34].

In the studies system, the locations of DG inverters and CBs are shown in Fig. 4. The capacity of DG inverters is 200 kW while the capacity of CBs is 300 kVar with 6 tap positions, each step corresponds to a step length of 50 kVar. The OLTC is operated in the range of ±5% with 20 tap positions, each step corresponds to a step length of 0.005 pu. The daily solar and load profile are obtained from Pecan Street [35] and NREL Data Center [36], respectively, which are shown in Figs. 5 and 6. The mean of ambiguity set D is the forecasting errors of solar power and is assumed to be zero, forecasting errors are independent so that the covariance matrix $\boldsymbol{\Sigma}$ is diagonal. The cost coefficient of power losses is chosen as 0.08 $/kWh while the cost coefficients of OLTC and CB operation are set as 1.40 $ and 0.24 $ per step [37].

4.2. Verification of prediction

One of the key advantages of the proposed TDRC-RHC is the capability of considering both the present and forecasted DG inverter generation to improve the performance. To demonstrate this, the total operation cost in 24-h simulation with prediction steps varying from 0 to 12 are summarized in Fig. 7. Initially, the cost is 132.32$ when only the current generation of DG inverters is considered. This number decreases to 107.53$ when the prediction step increasing to 6, which is a fairly improvement of 18.73% of the initial value. The number shows marginally difference when further extending the prediction horizon in this case.

4.3. Performance of TDRC-RHC

To illustrate the effectiveness of introducing chance constraint, 500 random Monto-Carlo samples are generated to observe the difference between deterministic optimization and the proposed TDRC-RHC. In deterministic optimization [8,38], the real renewable generation is assumed to strictly follow the forecasting value, the forecasting errors $\boldsymbol{\xi}$ are not taken into account, that is $\boldsymbol{p}_{\mathrm{inv}} = \overline{\boldsymbol{p}}_{\mathrm{inv}}$ in (10e) (12e). In addition, the voltage constraint in (10i) (12i) is changed into hard constraints, e.g. $\underline{\boldsymbol{u}} \leqslant \boldsymbol{u} \leqslant \overline{\boldsymbol{u}}$.

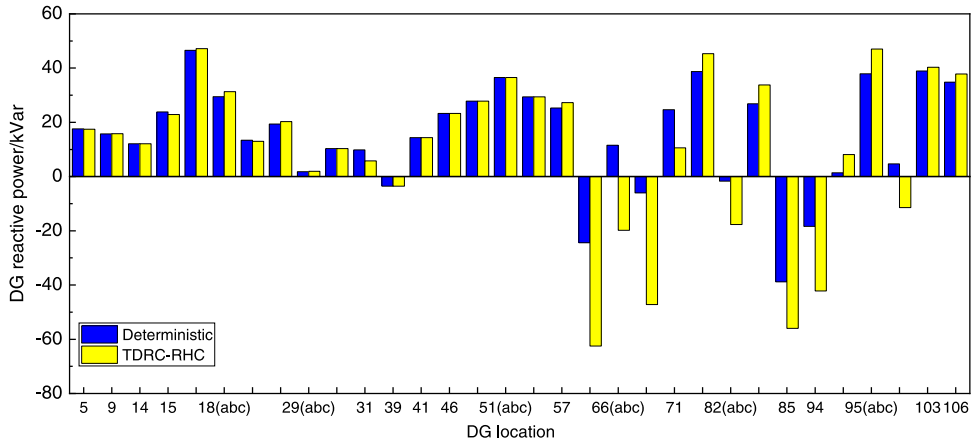

Fig. 13. DG reactive power outputs.

Table 1
TDRC-RHC and deterministic.

	Cost/$	Power losses/kWh	OLTC/times	CB/times
Deterministic	132.32	1348.59	13	26
TDRC-RHC	135.22	1390.74	13	24

Table 2
Probability violation in TDRC-RHC.

	$\epsilon = 0.01$	$\epsilon = 0.02$	$\epsilon = 0.05$
$\sigma = 0.05$	0.011	0.016	0.036
$\sigma = 0.1$	0.012	0.017	0.038
$\sigma = 0.2$	0.013	0.018	0.049

Table 3
Probability violation in scenario method.

	$\epsilon = 0.01$	$\epsilon = 0.02$	$\epsilon = 0.05$
$\sigma = 0.05$	0.011	0.016	0.036
$\sigma = 0.1$	0.013	0.017	0.040
$\sigma = 0.2$	0.014	0.019	0.050

The bus voltages of deterministic optimization at 10:00 is shown in Fig. 8. In Fig. 8, voltage violation happens in 268 scenarios, about 53.8% of the total scenarios. The most severe voltage violations happen in bus 66, 71 and 94. However, the voltage profiles are regulated into allowed range with the proposed TDRC-RHC as shown in Fig. 9.

The reason for the difference in Figs. 8 and 9 is that the proposed TDRC-RHC can guarantee the bus voltages within allowed limits in presence of uncertainties by introducing a safe margin. In this case, the reformulated voltage constraint is shown in Fig. 10 (to save space, we only list DG node here). It is slightly narrower than the original voltage hard constraint and different buses may have different voltage limits, while all the buses have the same voltage limit in deterministic optimization. The reformulated voltage constraint leads to different optimization results. We next show the results of VVC devices in these two methods as in Figs. 11–13. The tap positions of mechanical devices in these two methods are similar, the difference is that the tap positions of T1 Phase b in the proposed TDRC-RHC is slightly lower than that in deterministic optimization. As shown in Fig. 13, the reactive power outputs of most DG inverters are similar, except those located at bus 66, 71 and 94 absorb apparently more reactive power in the proposed TDRC-RHC. This is the main reason resulting in different voltage profiles between Figs. 8 and 9

To get a better overview of the two methods, the objective functions in deterministic optimization and the proposed TDRC-RHC are summarized in Table 1. Compared with deterministic optimization, the power losses and total operation cost in TDRC-RHC increase by 3.21% and 2.19%, respectively. This means that introducing chance constraint can guarantee the operation security, but the tightened voltage constraint makes the optimization result conservative thus increases cost. However, the cost increase is minimal and acceptable.

4.4. Comparison with scenario methods

Finally, we compare the performance of proposed TDRC-RHC and the scenario-based CC method. In scenario-based method, certain number of realization of uncertainty is generated. Then Monto-Carlo simulation is performed to determine the voltage probability distribution function around the forecasted point $\boldsymbol{u}_{0,i}$. After that, the upper $(1-\epsilon)$ and lower (ϵ) quantiles of the distribution can be determined. The safety margin in scenario method can be given as,

$$\lambda_{\max,i} = \boldsymbol{u}_i^{1-\epsilon} - \boldsymbol{u}_{0,i} \tag{24a}$$

$$\lambda_{\min,i} = \boldsymbol{u}_{0,i} - \boldsymbol{u}_i^{\epsilon} \tag{24b}$$

After the results of the TDRC-RHC and scenario method are obtained, we use 10 000 Monto-Carlo samples to verify the real violation probability in both methods. The maximum observed violation probability in two method is shown in Tables 2 and 3, respectively. From two tables, we can see the observed violation probability in two methods follows the pre-assumed one, also the results obtained in the proposed method are close to that in the scenario method, proving the accuracy of the proposed TDRC-RHC.

Finally the computation burden in two method is compared in this section. To this end, the minimum sample size in scenario approach needs to be determined. The allowed violation value of ϵ is set as 0.02 while the confidence parameter is chosen as 10^{-4}, this corresponding to a prescribed sample size of $N = 6323$ samples. Due to the large number of scenarios involved, the totally CPU time for solving USC is 4213 s and 821 s for LSC in scenario method. However, it only takes 0.92 s to solve USC problem and 0.15 s to solve LSC in the proposed TDRC-RHC, demonstrating the superiority of the proposed method.

5. Conclusion

This paper proposed a two-stage distributionally robust chance-constrained receding horizon voltage control method to address the voltage control problem in distribution networks caused by high penetration of renewable generation. By taking into the forecasting renewable generation into consideration, the proposed method can achieve an improvement of 18.73% using the idea of receding horizon control.

Case studies on IEEE-123 bus systems show that the proposed method are robust to uncertainty renewable generation, whereas the voltage violation happens under more than 50% scenarios in deterministic optimization. In addition, the proposed method can significantly reduce the computation burden (e.g. 0.92 s to solve USC and 0.15 s for LSC whereas these figures in scenario method are 4231 s and 821 s) while guarantee the accuracy at the same time.

Currently ambiguity set defined by first and second moment is used to model the forecasting errors of renewable generation, however, the higher order moment information is ignored. In addition, the moment-based ambiguity set covers all the probability distributions sharing the known moment information, there might be the possibility of containing some unrealistic distributions that make the solution conservative. In future work, modeling uncertainty forecasting errors by combined ambiguity set or data-driven method to overcome above limitations will be explored.

Declaration of competing interest

The authors declare that they have no known competing financial interests or personal relationships that could have appeared to influence the work reported in this paper.

References

[1] N. Mahmud, A. Zahedi, Review of control strategies for voltage regulation of the smart distribution network with high penetration of renewable distributed generation, Renew. Sustain. Energy Rev. 64 (2016) 582–595.

[2] H. Sadeghian, Z. Wang, A novel impact-assessment framework for distributed PV installations in low-voltage secondary networks, Renew. Energy 147 (2020) 2179–2194.

[3] K. Turitsyn, P. Šulc, S. Backhaus, M. Chertkov, Distributed control of reactive power flow in a radial distribution circuit with high photovoltaic penetration, in: IEEE PES General Meeting, IEEE, 2010, pp. 1–6.

[4] F. Ferdowsi, S. Mehraeen, G.B. Upton Jr., Assessing distribution network sensitivity to voltage rise and flicker under high penetration of behind-the-meter solar, Renew. Energy 152 (2020) 1227–1240.

[5] D.G. Photovoltaics, E. Storage, IEEE standard for interconnection and interoperability of distributed energy resources with associated electric power systems interfaces, in: IEEE Std, 2018, pp. 1547–2018.

[6] S.M. Mohseni-Bonab, A. Rabiee, B. Mohammadi-Ivatloo, Voltage stability constrained multi-objective optimal reactive power dispatch under load and wind power uncertainties: A stochastic approach, Renew. Energy 85 (2016) 598–609.

[7] Z. Wang, J. Wang, B. Chen, M.M. Begovic, Y. He, MPC-based voltage/var optimization for distribution circuits with distributed generators and exponential load models, IEEE Trans. Smart Grid 5 (5) (2014) 2412–2420.

[8] Y. Xu, Z.Y. Dong, R. Zhang, D.J. Hill, Multi-timescale coordinated voltage/var control of high renewable-penetrated distribution systems, IEEE Trans. Power Syst. 32 (6) (2017) 4398–4408.

[9] E. Delage, Y. Ye, Distributionally robust optimization under moment uncertainty with application to data-driven problems, Oper. Res. 58 (3) (2010) 595–612.

[10] T. Ding, C. Li, Y. Yang, J. Jiang, Z. Bie, F. Blaabjerg, A two-stage robust optimization for centralized-optimal dispatch of photovoltaic inverters in active distribution networks, IEEE Trans. Sustain. Energy 8 (2) (2016) 744–754.

[11] H. Gao, J. Liu, L. Wang, Robust coordinated optimization of active and reactive power in active distribution systems, IEEE Trans. Smart Grid 9 (5) (2017) 4436–4447.

[12] C. Zhang, Y. Xu, Z.Y. Dong, R. Zhang, Multi-objective adaptive robust voltage/VAR control for high-PV penetrated distribution networks, IEEE Trans. Smart Grid 11 (6) (2020) 5288–5300.

[13] T. Xu, Y. Ren, L. Guo, X. Wang, L. Liang, Y. Wu, Multi-objective robust optimization of active distribution networks considering uncertainties of photovoltaic, Int. J. Electr. Power Energy Syst. 133 (2021) 107197.

[14] D. Bertsimas, D.B. Brown, C. Caramanis, Theory and applications of robust optimization, SIAM Rev. 53 (3) (2011) 464–501.

[15] H. Zhang, P. Li, Chance constrained programming for optimal power flow under uncertainty, IEEE Trans. Power Syst. 26 (4) (2011) 2417–2424.

[16] F.U. Nazir, B.C. Pal, R.A. Jabr, A two-stage chance constrained volt/var control scheme for active distribution networks with nodal power uncertainties, IEEE Trans. Power Syst. 34 (1) (2018) 314–325.

[17] T. Yang, Y. Yu, Steady-state security region-based voltage/var optimization considering power injection uncertainties in distribution grids, IEEE Trans. Smart Grid 10 (3) (2018) 2904–2911.

[18] Y. Jiang, C. Wan, J. Wang, Y. Song, Z.Y. Dong, Stochastic receding horizon control of active distribution networks with distributed renewables, IEEE Trans. Power Syst. 34 (2) (2018) 1325–1341.

[19] B.A. Robbins, A.D. Domínguez-García, Optimal reactive power dispatch for voltage regulation in unbalanced distribution systems, IEEE Trans. Power Syst. 31 (4) (2015) 2903–2913.

[20] Y. Guo, Q. Zhang, Z. Wang, F. Bu, Y. Yuan, Two-layer volt/VAR control in unbalanced active distribution systems: Efficient optimization and accurate tracking, 2019, arXiv preprint arXiv:1912.11173.

[21] R.B. Bapat, Graphs and Matrices, Vol. 27, Springer, 2010.

[22] Y. Kim, N.-G. Myoung, S.-Y. Lee, Study on AMI system of KEPCO, in: 2010 International Conference on Information and Communication Technology Convergence (ICTC), IEEE, 2010, pp. 459–460.

[23] M.Y. Nguyen, Optimal voltage controls of distribution systems with OLTC and shunt capacitors by modified particle swarm optimization: A case study, AIMS Energy 7 (6) (2019) 883–900.

[24] L. Blakely, M.J. Reno, K. Ashok, AMI data quality and collection method considerations for improving the accuracy of distribution models, in: 2019 IEEE 46th Photovoltaic Specialists Conference (PVSC), IEEE, 2019, pp. 2045–2052.

[25] V.N. Lal, M. Siddhardha, S. Singh, Control of a large scale single-stage grid-connected PV system utilizing MPPT and reactive power capability, in: 2013 IEEE Power & Energy Society General Meeting, IEEE, 2013, pp. 1–5.

[26] A.M. Howlader, S. Sadoyama, L.R. Roose, S. Sepasi, Distributed voltage regulation using volt-var controls of a smart PV inverter in a smart grid: An experimental study, Renew. Energy 127 (2018) 145–157.

[27] J. Li, C. Liu, M.E. Khodayar, M.-H. Wang, Z. Xu, B. Zhou, C. Li, Distributed online VAR control for unbalanced distribution networks with photovoltaic generation, IEEE Trans. Smart Grid 11 (6) (2020) 4760–4772.

[28] M. Nick, R. Cherkaoui, M. Paolone, Optimal allocation of dispersed energy storage systems in active distribution networks for energy balance and grid support, IEEE Trans. Power Syst. 29 (5) (2014) 2300–2310.

[29] M.C. Campi, S. Garatti, M. Prandini, The scenario approach for systems and control design, Annu. Rev. Control 33 (2) (2009) 149–157.

[30] L.A. Roald, Optimization Methods to Manage Uncertainty and Risk in Power Systems Operation (Ph.D. thesis), ETH Zurich, 2016.

[31] H. Acikgoz, A novel approach based on integration of convolutional neural networks and deep feature selection for short-term solar radiation forecasting, Appl. Energy 305 (2022) 117912.

[32] G.C. Calafiore, L. El Ghaoui, On distributionally robust chance-constrained linear programs, J. Optim. Theory Appl. 130 (1) (2006) 1–22.

[33] IEEE distribution test feeder, 2017, URL https://cmte.ieee.org/pes-testfeeders/.

[34] L. Gurobi Optimization, Gurobi optimizer reference manual, 2020, URL http://www.gurobi.com.

[35] Dataport, 2017, URL https://www.pecanstreet.org/.

[36] Solar power data, 2020, URL https://www.nrel.gov/grid/solar-power-data.html.

[37] P. Li, H. Ji, C. Wang, J. Zhao, G. Song, F. Ding, J. Wu, Coordinated control method of voltage and reactive power for active distribution networks based on soft open point, IEEE Trans. Sustain. Energy 8 (4) (2017) 1430–1442.

[38] T. Ding, S. Liu, W. Yuan, Z. Bie, B. Zeng, A two-stage robust reactive power optimization considering uncertain wind power integration in active distribution networks, IEEE Trans. Sustain. Energy 7 (1) (2015) 301–311.